

Indication of a Differential Freeze-out in Proton-Proton and Heavy-Ion Collisions at RHIC and LHC energies

Dhananjaya Thakur, Sushanta Tripathy, Prakhar Garg*, and Raghunath Sahoo†
*Discipline of Physics, School of Basic Sciences, Indian Institute of Technology Indore,
 Khandwa Road, Simrol, Madhya Pradesh- 453552, India.*

Jean Cleymans
*UCT-CERN Research Centre and Department of Physics,
 University of Cape Town, Rondebosch 7701, South Africa
 (Dated: November 22, 2016)*

The experimental data from the RHIC and LHC experiments of invariant p_T spectra for most peripheral A+A and $p+p$ collisions are analyzed with Tsallis distributions in different approaches. The information about the freeze-out surface in terms of freeze-out volume, temperature, chemical potential and radial flow velocity for π^+ , K^+ , p and their anti-particles are obtained. Further, these parameters are studied as a function of the mass of the particles. A mass-dependent differential freeze-out is observed which does not seem to distinguish between particles and their antiparticles. Furthermore, a mass-hierarchy in the radial flow is observed, meaning heavier particles suffer lower radial flow. Tsallis distribution function at finite chemical potential is used to study the mass dependence of chemical potential. The peripheral heavy-ion and proton-proton collisions at the same energies seem to be equivalent in terms of the extracted thermodynamic parameters.

PACS numbers:

I. INTRODUCTION

High-energy heavy ion collisions provide an unique opportunity to study the nuclear matter under extreme conditions i.e. at high temperature and/or density. Due to high multiplicities produced in A+A and $p+p$ collisions, the statistical models are more suitable to describe the particle production mechanism. Such a statistical description of transverse momentum (p_T) of final state particles produced in high-energy collisions has been proposed to follow a thermalized Boltzmann type of distribution as given by [1]

$$E \frac{d^3\sigma}{d^3p} \simeq C \exp\left(-\frac{p_T}{T_{exp}}\right). \quad (1)$$

To account for the high- p_T tail, a power-law in p_T has been proposed [2, 3], which empirically accounts for the possible QCD contributions. Hagedorn proposed a combination of both the aspects, which describes the experimental data over a wide p_T range [4] and is given by

$$\begin{aligned} E \frac{d^3\sigma}{d^3p} &= C \left(1 + \frac{p_T}{p_0}\right)^{-n} \\ &\longrightarrow \begin{cases} \exp\left(-\frac{np_T}{p_0}\right) & \text{for } p_T \rightarrow 0, \\ \left(\frac{p_0}{p_T}\right)^n & \text{for } p_T \rightarrow \infty, \end{cases} \end{aligned} \quad (2)$$

where C , p_0 , and n are fitting parameters. This becomes a purely exponential function for small p_T and a purely power-law function for large p_T values. A finite degree of deviation from the equilibrium statistical description of identified particle p_T spectra has already been observed by experiments at RHIC [5, 6] and LHC [7–10]. Contrary to a thermalized system, where the $\langle p_T \rangle$ is associated with the temperature of the hadronizing matter, one fails to make such a connection in case of systems which are far from thermal equilibrium. In the latter systems, either the temperature fluctuates event by event or within the same event [11]. This creates room for possible description of the p_T spectra in high-energy hadronic and nuclear collisions, using the non-extensive Tsallis statistics [12–14]. A thermodynamically consistent non-extensive distribution function is given by [15]

$$f(m_T) = C_q \left[1 + (q-1) \frac{m_T}{T}\right]^{-\frac{1}{q-1}}. \quad (3)$$

Here, m_T is the transverse mass and q is called the non-extensive parameter- a measure of degree of deviation from equilibrium. Eqs. 2 and 3 are related through the following transformations for large values of p_T :

$$n = \frac{1}{q-1}, \text{ and } p_0 = \frac{T}{q-1}. \quad (4)$$

In the limit $q \rightarrow 1$, one recovers the standard Boltzmann-Gibbs distribution (Eq. 1) from the Tsallis distribution (Eq. 6). Here the effective kinetic freeze-out temperature (T_{exp}) as obtained from the inverse slope of the p_T -spectra using Eq. 1, is related to the Tsallis temperature (T) by

$$T_{exp} \simeq a + b.T, \quad (5)$$

*Current Affiliation: Department of Physics and Astronomy, Stony Brook University, SUNY, Stony Brook, New York 11794-3800, USA

†Corresponding author: *Raghunath.Sahoo@cern.ch*

where $a = 0.31 - 0.654 q + 0.354 q^2$ and $b = 27.35 - 55 q + 29.07 q^2$ and are obtained numerically for distributions with same mean transverse momentum, $\langle p_T \rangle$, as discussed in Ref. [51] for $p + p$ collisions in the low- p_T ($0.15 < p_T < 0.6$ GeV/c) regime.

Tsallis statistics is used widely to explain the particle spectra in high energy collisions [11, 16–21] starting from elementary $e^+ + e^-$, hadronic and heavy-ion collisions [22–39]. The produced particles from the collisions carry the information about collision dynamics and the subsequent space-time evolution till the occurrence of the final freeze-out. The evolution of the partonic system created in high energy experiments is generally believed to be best described by hydrodynamics of an almost ideal fluid [40]. This approach gives a fair description of data on the transverse momentum spectra of hadrons, which are treated as one of the important tools to understand the production dynamics of particles in high-energy collisions. The systematic analysis with the help of an appropriate model or approach guides us to understand various thermodynamical as well as hydrodynamical properties of the fireball at different stages of its evolution. The integrated yields of various hadronic species at different center of mass energies are used in the present work. The corresponding freeze-out parameters for each hadronic species at the time of their freeze-out can be obtained from the analysis of their respective transverse momentum distributions. Different forms of the invariant yields using Tsallis distribution are available in the literature [18, 41, 42]. In the present work we have used all of these forms to study the temperature (T), chemical potential (μ), radial flow (β), volume (V) and non-extensive parameter (q). It should be mentioned here that the parameter V is not necessarily related to the volume one obtains from HBT like experimental measurements. Further, we study the mass dependence of these parameters, which are obtained by analyzing invariant transverse momentum spectra. For the present analysis, we have used the data of $p + p$ and A+A collisions of different experiments at RHIC and LHC. We observe a clear mass dependence of the above parameters, and the behaviour is found to be consistent from most peripheral A+A collisions to $p + p$ collisions. The obtained thermodynamic parameters in $p + p$ collisions are similar to those extracted for most peripheral A+A collisions at the same centre of mass energies. This indicates a thermodynamical similarity between both the systems at a given collision energy.

In the heavy ion collision, the interaction volume of fireball decreases from most central to most peripheral collisions. So the number of participant nucleons also decreases from most central collisions to most peripheral collisions depending on the interaction volume. The system having more participant will quickly reach the equilibrium because of large number of binary collisions by rescattering of partons/hadrons as can be the case in central A+A collisions. But in case of peripheral collisions due to smaller number of participant the system will be

away from equilibrium for a while as compared to central collisions. Such a non equilibrium system is better described by Tsallis non-extensive statistics, giving information about the various thermodynamic parameters of the system.

The paper is organized as follows. In section 2, we present three forms of Tsallis distribution functions. Firstly, we discuss invariant yields with and without chemical potential in the Tsallis function. Then we show the Tsallis form of invariant yields with radial flow which is introduced analytically in one of our recent works [18]. In section 3, results and discussions are made. Lastly, we conclude our findings in section 4.

II. NON-EXTENSIVITY AND TRANSVERSE MOMENTUM SPECTRA

In the following sections, we discuss the transverse momentum spectra of identified particles (π^+ , K^+ , p and their antiparticle) produced in RHIC and LHC experiments using different forms of invariant yields using Tsallis non-extensive statistics.

A. Non-extensive statistics without radial flow

The Tsallis distribution function at mid-rapidity, with finite chemical potential and without radial flow [41] is given by,

$$\frac{1}{p_T} \frac{d^2 N}{dp_T dy} \Big|_{y=0} = \frac{g V m_T}{(2\pi)^2} \left[1 + (q-1) \frac{m_T - \mu}{T} \right]^{-\frac{q}{q-1}} \quad (6)$$

where, m_T is the transverse mass of a particle given by $\sqrt{p_T^2 + m^2}$, g is the degeneracy and μ is the chemical potential of the system. In view of higher center of mass energies, where $\mu \simeq 0$, the transverse momentum distribution function [42] becomes:

$$\frac{1}{p_T} \frac{d^2 N}{dp_T dy} \Big|_{y=0} = \frac{g V m_T}{(2\pi)^2} \left[1 + (q-1) \frac{m_T}{T} \right]^{-\frac{q}{q-1}}. \quad (7)$$

B. Non-extensive statistics with radial flow

The value of the non-extensive parameter q for high energy collisions is $1 \leq q \leq 1.2$ [43]. To study the order of deviation of the p_T -spectra from a equilibrium Boltzmann distribution, the Tsallis distribution function has been expanded in a Taylor series in view of $(q-1)$ being very small, after successful inclusion of radial flow in a relativistic scenario. The details of the method are described in Ref. [18]. The functional form of the distri-

bution up to first order in $(q - 1)$ is given by

$$\frac{1}{2\pi p_T} \frac{dN}{dp_T dy} = \frac{gV}{(2\pi)^3} \left\{ 2T[rI_0(s)K_1(r) - sI_1(s)K_0(r)] - (q-1)Tr^2I_0(s)[K_0(r) + K_2(r)] + 4(q-1)TrsI_1(s)K_1(r) - (q-1)Ts^2K_0(r)[I_0(s) + I_2(s)] + \frac{(q-1)}{4}Tr^3I_0(s)[K_3(r) + 3K_1(r)] - \frac{3(q-1)}{2}Tr^2s[K_2(r) + K_0(r)]I_1(s) + \frac{3(q-1)}{2}Ts^2r[I_0(s) + I_2(s)]K_1(r) - \frac{(q-1)}{4}Ts^3[I_3(s) + 3I_1(s)]K_0(r) \right\} \quad (8)$$

where, $r \equiv \frac{\gamma m_T}{T}$, $s \equiv \frac{\gamma \beta p_T}{T}$. $I_n(s)$ and $K_n(r)$ are the modified Bessel functions of the first and second kind. There are four parameters involved namely V , T , β and q ; where V is the volume, T is the Tsallis temperature, β is the radial flow velocity and q is the Tsallis non-extensive parameter.

We use Eq. 8 to fit the particle spectra of identified particles in heavy ion collisions to study the radial flow parameter.

III. RESULTS AND DISCUSSION

It is expected that the number of binary collisions in a system with smaller number of participant nucleons is quite low. Hence, the probability of mutual interaction (resulting in momentum transfer) between the system quanta- partons or hadrons, becomes less for the systems with small value of participating nucleons. This makes the system to stay away from a possible thermal equilibrium. On the other hand, an appreciable increment in the number of binary collisions is observed in a system possessing a large number of participant nucleons and consequently the system can reach quickly to its thermal equilibrium or in the close vicinity of it. It has been shown in Ref.[44], that the non-extensivity parameter (q) is close to 1 in central Au+Au collisions and increases towards peripheral collisions. A higher value of q reflects that the system is away from thermal equilibrium. These results suggest that the degree of non-equilibrium is higher in peripheral collisions. Such systems are best described by Tsallis distributions for example the most peripheral A+A and p+p systems. We perform the fitting of p_T spectra for $p_T < 3$ GeV/c around mid rapidity at $\sqrt{s_{NN}} = 200$ GeV and $\sqrt{s_{NN}} = 2.76$ TeV. Keeping all the parameters free, we try to fit the spectra with Eqns. 6, 7 and 8 independently for different particles like π^+ , K^+ , p and their antiparticle for Pb+Pb and Au+Au

most peripheral collisions using TMinuit class available in the ROOT library[45] to get a convergent solution. The same procedure is followed for $p + p$ collisions as well.

We have discussed the present work in three sections. Now, Eq. 7 is used to analyze invariant p_T spectra of identified particles (π^+ , K^+ , p and their antiparticles) for most peripheral Au+Au collisions at $\sqrt{s_{NN}} = 200$ GeV and most peripheral Pb+Pb collisions at $\sqrt{s_{NN}} = 2.76$ TeV along with $p + p$ collisions at both energies. The fitting of p_T spectra of identified particles for Au+Au collisions at 200 GeV and Pb+Pb collisions at 2.76 TeV are shown in Figs. 11 and 12 (in Appendix) for most peripheral collisions. Also, Figs. 13 and 14 of appendix section show the fitting of invariant spectra to $p + p$ collisions at 200 GeV and 2.76 TeV, respectively for identified particles. The fitting is performed up to the maximum p_T of 3 GeV/c for A+A collisions and 2.5 GeV/c for $p + p$ collisions although the K^+ p_T spectra in Au+Au collision is fitted only up-to 2.0 GeV/c due to unavailability of data [46]. The fittings of Tsallis function with $\mu = 0$ seem to be better for peripheral heavy-ion collisions. The χ^2/ndf obtained by minimization in TMinuit are shown in Figs. 1 and 2.

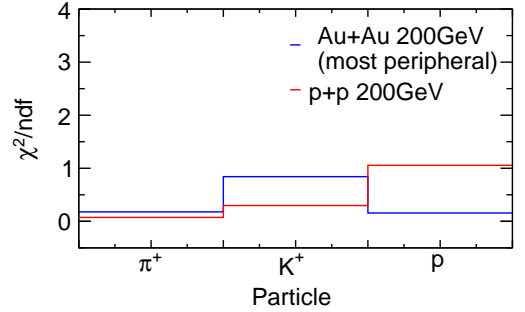


FIG. 1: (color online) χ^2/ndf values are shown for most peripheral Au+Au and $p + p$ collisions at $\sqrt{s_{NN}} = 200$ GeV using Eq. 7 as a fit function.

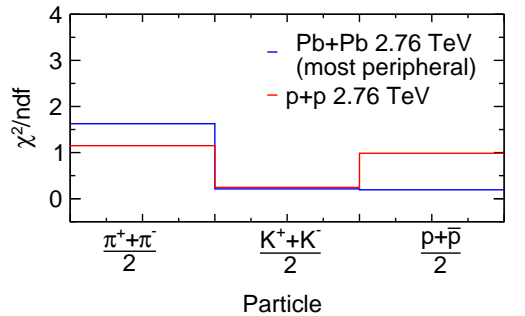


FIG. 2: (color online) χ^2/ndf values are shown for most peripheral Pb+Pb and $p + p$ collisions at $\sqrt{s_{NN}} = 2.76$ TeV using Eq. 7 as a fit function.

A systematic study of the extracted parameters like

volume (V), temperature (T) and Tsallis non-extensive parameter (q), is made with identified particle masses. The values of extracted parameters are summarized in Table. I of the appendix. We have calculated the radius of the fireball at freeze-out and plotted as a function of the mass of the identified particles. Figures 3 and 4 show the variation of common mass dependent parameters at $\sqrt{s_{NN}} = 200$ GeV and $\sqrt{s_{NN}} = 2.76$ TeV. We have then compared the parameters obtained for peripheral heavy-ion collisions with that of $p + p$ collisions at the same centre of mass energies to understand the thermodynamic properties of the produced systems.

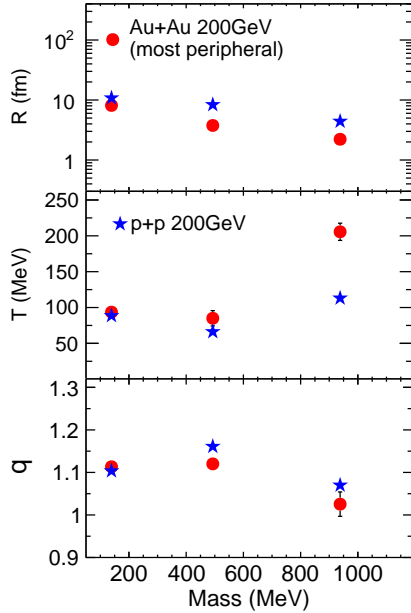


FIG. 3: (color online) Mass dependence of the thermodynamic parameters using Eq. 7 for most peripheral Au+Au and $p + p$ collisions at $\sqrt{s_{NN}} = 200$ GeV.

It is found that the volume parameter decreases with increase in particle mass. It indicates that different particles have different freeze-out surfaces depending on their mass. This is observed both for $p + p$ and A+A collisions and thus indicates a mass dependent differential freeze-out scenario in high-energy collisions. In view of the above freeze-out picture, taking T as the freeze-out temperature, we observe from Figs. 3 and 4 that the freeze-out temperature slightly increases with particle mass. This observation goes inline with the earlier findings of Ref. [47], which uses a slightly different approach. It clearly indicates that the heavier particles have higher freeze-out temperature as compared to lighter particles. This observation goes in-line with an intuitive expectation of mass dependent particle freeze-out or differential freeze-out. In literature, one finds various freeze-out scenarios like, single freeze-out [20], strange and non-strange particles having two different freeze-outs [52, 53] etc. However, our findings from the analysis of

high-energy particle spectra with non-extensive statistics reveals a consistent differential freeze-out scenario with particles and their counter parts, the anti-particles freezing out at the same time (characterized by freeze-out temperature, freeze-out volume) from the produced fireballs. The non-extensive measure i.e., the q -parameter obtained from our studies is consistent with its value, $1 < q < 1.2$, both for $p + p$ and A+A collisions. This goes in-line with the expectations of the q -values in high-energy collisions [43].

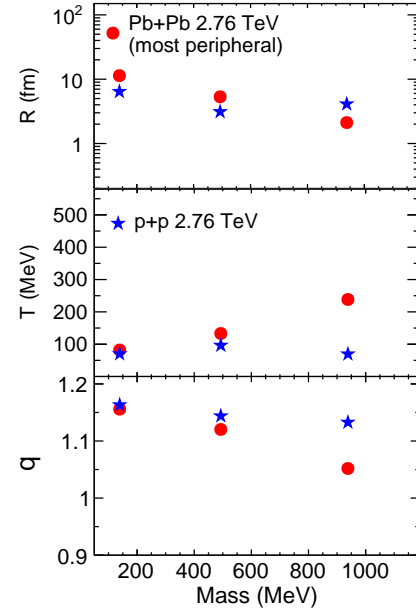


FIG. 4: (color online) Mass dependence of thermodynamic parameters using Eq. 7 for most peripheral Pb+Pb and $p + p$ collisions at $\sqrt{s_{NN}} = 2.76$ TeV.

Also, Figs. 3 and 4 indicate a similar mass ordering for $p + p$ systems, which indicates that the system formed in most peripheral A+A collisions and $p + p$ collisions are of similar thermodynamic nature. However, it should be noted that the obtained parameters seem to be unphysical i.e. volume or the radius in $p + p$ collisions seem to be higher than the peripheral A+A collisions at the same energy. This problem is observed to be circumvented, when one adds the radial flow to the distribution. This is seen in the subsequent discussions and in Table-III.

Secondly, we perform the fitting of invariant p_T spectra of identified particles using Eq. 6 which contains an additional parameter as chemical potential (μ). The same fitting procedure is used to fit Au+Au most peripheral collisions at $\sqrt{s_{NN}} = 200$ GeV for identified particles as well as their antiparticles. The Tsallis form of invariant yields including μ is used in Fig. 15. It fits up to $p_T \sim 3$ GeV/c for most peripheral collisions. The goodness of fit can be seen from χ^2/ndf values shown in Figure 5.

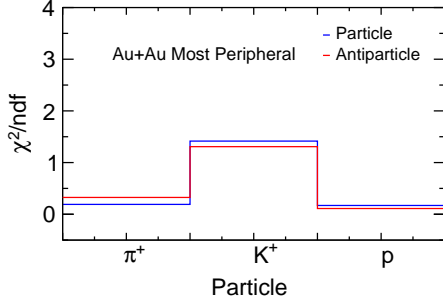


FIG. 5: (color online) χ^2/ndf values are shown for most peripheral Au+Au collisions at $\sqrt{s_{NN}} = 200$ GeV using Eq. 6 as a fit function.

The mass dependence of extracted parameters are shown in the Figure 6. Also, the values of the parameters are tabulated in Table. II of the appendix. In Figure 6, it is shown that all the parameters follow the same mass dependent trend as is discussed in the previous cases. Besides, an additional parameter, chemical potential (μ), is shown.

It is to be mentioned here that, the chemical potential is extracted from the invariant yields at the thermal freeze out, where all the elastic processes cease. Hence the obtained chemical potential here is called thermal chemical potential. At this stage one can introduce chemical potentials for all particle species (μ_i). Following Ref. [50], the relationship between chemical potential at kinetic freeze-out and chemical potential at chemical freeze-out is given by

$$\mu_{th} = \mu_{ch} \frac{T_{th}}{T_{ch}} + m(1 - \frac{T_{th}}{T_{ch}}) \quad (9)$$

Where (T_{ch}, T_{th}) and (μ_{ch}, μ_{th}) are temperature and chemical potential at chemical and thermal freeze out respectively. Eq.9 clearly shows a mass dependency of thermal chemical potential.

The extracted parameters shown in Fig. 6 shows a consistent picture for particles and antiparticles in case of most peripheral collisions. It is evident from Fig. 6 that the μ -parameter increases with particle mass. It shows that particles and antiparticles have same freeze-out conditions. It is worth mentioning here that the parameters T and μ extracted from identified particle spectra using Eqn. 6 are related by [51]

$$T = T_0 + (q - 1)\mu, \quad (10)$$

where $T = T_0$ for $\mu = 0$. Our extracted parameters using Eqns. 6 (i.e. T, μ and q) and 7 (i.e. $T \equiv T_0$) seem to obey the above relation.

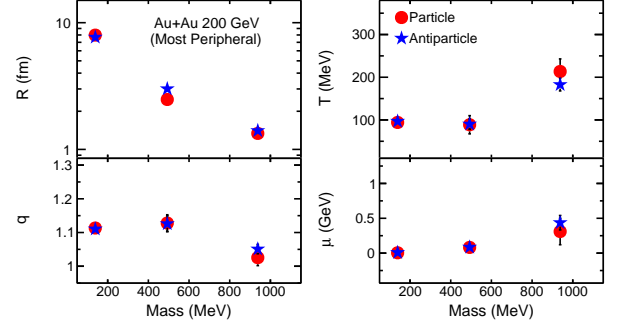


FIG. 6: (color online) Mass dependence of extracted thermodynamic parameters using Eq.6 for different particles and their corresponding antiparticles for most peripheral Au+Au collisions at $\sqrt{s_{NN}} = 200$ GeV.

Finally, the invariant p_T spectra of identified particles is fitted with Eq. 8 for most peripheral collisions of Au+Au at $\sqrt{s_{NN}} = 200$ GeV and Pb+Pb at $\sqrt{s_{NN}} = 2.76$ TeV. Besides, the fitting of identified particles for $p + p$ collisions is done for same energies. The fitting results for Au+Au collisions at $\sqrt{s_{NN}} = 200$ GeV and the results for Pb+Pb collisions at $\sqrt{s_{NN}} = 2.76$ TeV are shown in Figs. 16 and 17, respectively. Also, the fitting results for $p + p$ collisions at $\sqrt{s_{NN}} = 200$ GeV and $\sqrt{s_{NN}} = 2.76$ TeV are shown in Figs. 18 and 19, respectively in the appendix section.

The fitting is performed up to $p_T \sim 3$ GeV/c in A+A collisions and $p_T \sim 2.5$ GeV/c in $p + p$ collisions, only a slight deviation at higher p_T is observed in pion spectra. The values of various parameters obtained from the fits are provided in Table. III. It is observed from the values of χ^2/ndf (Table. III) that the performance of the present approach is quite satisfactory, except in case of pion, which can be seen from the Figs. 7 and 8.

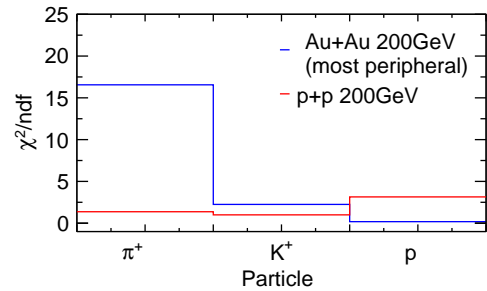


FIG. 7: (color online) χ^2/ndf values are shown for most peripheral Au+Au collision and $p + p$ collisions at $\sqrt{s_{NN}} = 200$ GeV using Eq. 8 as a fit function.

Then we make a mass dependent study of these parameters. Figs. 9 and 10 represent the behaviour of the extracted parameters. The parameters like volume, tem-

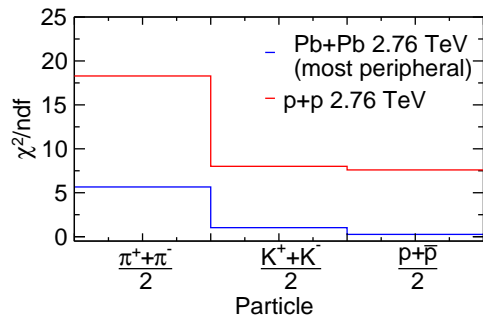


FIG. 8: (color online) χ^2/ndf values are shown for most peripheral Pb+Pb collisions and $p + p$ collisions at $\sqrt{s_{NN}} = 2.76$ TeV using Eq. 8 as a fit function.

perature and q show a similar mass dependent behaviour as that of the parameters obtained from the fitting using Eq. 6 and Eq. 7. Here, through Eq. 8, we have introduced an additional radial flow parameter (β). Figs. 9 and 10 show the decrease of radial flow with increase of particle mass, which is a signature of hydrodynamic evolution of the system created in high energy collisions. The change of temperature parameter with the use of different forms of Tsallis distribution could be observed in Ref.[54]. In our analysis we have also observed not only the temperature but also the other parameters are changing with the use of different forms of Tsallis distributions. For example, it is observed that with the inclusion of radial flow, the value of the q -parameter becomes less, as compared to that observed in the other forms of Tsallis distribution, while describing the p_T -spectra. This may hint that the non-extensivity is shared by the dynamics of the system[55–57].

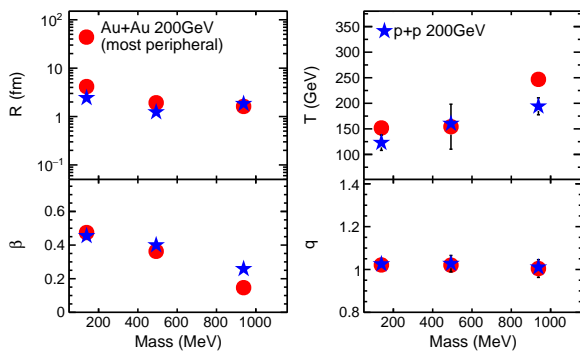


FIG. 9: (color online) Mass dependence of extracted thermodynamic parameters of Tsallis distribution including radial flow using Eq. 8 for most peripheral Au+Au collisions and $p + p$ collisions at $\sqrt{s_{NN}} = 200$ GeV.

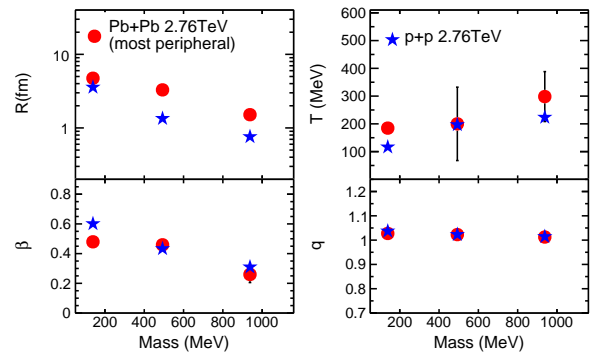


FIG. 10: (color online) Mass dependence of extracted thermodynamic parameters of Tsallis distribution including radial flow using Eq. 8 for most peripheral Pb+Pb collisions and $p + p$ collisions at $\sqrt{s_{NN}} = 2.76$ TeV.

IV. CONCLUSION

We present a systematic study of the parameters extracted from transverse momentum spectra of produced identified particles in Au+Au collisions at $\sqrt{s_{NN}} = 200$ GeV and Pb+Pb collisions at $\sqrt{s_{NN}} = 2.76$ TeV. Further, the same analysis is done for $p + p$ collisions at both, RHIC and LHC energies. In the present work different forms of invariant yields using Tsallis distribution are used. Parameters obtained from three different forms in most peripheral Au+Au collisions at $\sqrt{s_{NN}} = 200$ GeV and in most peripheral Pb+Pb collisions at $\sqrt{s_{NN}} = 2.76$ TeV follow a similar trend. Similar behaviour has been observed in $p + p$ collisions for both the energies. The chemical potential plays an important role in particle production mechanism. We observe that the particles produced at early stage have higher thermal chemical potential as compared to particles produced at the later stage. The radial flow extracted from the particle spectra of peripheral A+A collisions is similar to $p + p$ collisions at the same center of mass energy. In the discussed low- p_T region, the radial flow decreases with increasing mass, which goes in line with hydrodynamic description of the evolution of a fireball created in high-energy collisions. Therefore, the present analysis gives a systematic information of hydrodynamical and thermodynamical evolution of the system, while making a direct comparison with hadronic and peripheral nuclear collisions. We observe a mass dependent differential freeze-out scenario in high-energy hadronic and nuclear collisions, which is also supported by similar observations by other authors [58].

Acknowledgements

D.Thakur acknowledges the financial support from U.G.C, New Delhi and S. Tripathy acknowledges the

DST-INSPIRE scheme of Govt. of India for financial support.

V. APPENDIX

TABLE I: χ^2/ndf and different extracted parameters from Tsallis distribution fit(Eq. 7) to the p_T spectra of (a) π^+ , K^+ and p for most peripheral Au+Au collisions and $p + p$ collisions at $\sqrt{s_{NN}} = 200$ GeV; (b) $\frac{\pi^+ + \pi^-}{2}$, $\frac{K^+ + K^-}{2}$ and $\frac{p + \bar{p}}{2}$ for most peripheral Pb+Pb collisions and $\frac{\pi^+ + \pi^-}{2}$, $\frac{K^+ + K^-}{2}$ and $\frac{p + \bar{p}}{2}$ for $p + p$ collisions at $\sqrt{s_{NN}} = 2.76$ TeV.

Au+Au 200 GeV (Peripheral)				
Particle	χ^2/ndf	$V (fm)^3$	$T (GeV)$	q
π^+	0.178	2242.35 ± 18.23	0.093 ± 0.003	1.113 ± 0.004
K^+	0.842	223.358 ± 0.010	0.085 ± 0.011	1.120 ± 0.002
p	0.157	45.62 ± 2.45	0.205 ± 0.012	1.025 ± 0.029
$p + p$ 200 GeV				
π^+	0.073	5293.1 ± 23.3	0.088 ± 0.004	1.103 ± 0.005
K^+	0.297	2443.7 ± 33.7	0.066 ± 0.002	1.161 ± 0.009
p	1.055	360.5 ± 9.6	0.113 ± 0.004	1.070 ± 0.000

(a)

Pb+Pb 2.76 TeV (Peripheral)				
Particle	χ^2/ndf	$V (fm)^3$	$T (GeV)$	q
$\frac{\pi^+ + \pi^-}{2}$	1.626	6134.30 ± 12.61	0.082 ± 0.001	1.156 ± 0.002
$\frac{K^+ + K^-}{2}$	0.211	629.69 ± 14.80	0.133 ± 0.003	1.120 ± 0.004
$\frac{p + \bar{p}}{2}$	0.193	39.623 ± 1.052	0.238 ± 0.012	1.052 ± 0.009
$p + p$ 2.76 TeV				
$\frac{\pi^+ + \pi^-}{2}$	0.985	1102.46 ± 6.82	0.070 ± 0.001	1.163 ± 0.001
$\frac{K^+ + K^-}{2}$	0.094	127.13 ± 1.33	0.096 ± 0.005	1.144 ± 0.005
$\frac{p + \bar{p}}{2}$	0.006	291.39 ± 10.62	0.069 ± 0.003	1.133 ± 0.002

(b)

TABLE II: χ^2/ndf and different extracted parameters from Tsallis distribution fit(Eq. 6) to the p_T spectra of π^\pm , K^\pm , p and \bar{p} for most peripheral Au+Au collisions at $\sqrt{s_{NN}} = 200$ GeV.

Au+Au 200 GeV (Peripheral)					
Particle	χ^2/ndf	$V (fm)^3$	$T (GeV)$	q	$\mu (GeV)$
π^+	0.191	2125.93 ± 56.06	0.094 ± 0.004	1.113 ± 0.004	0.0050 ± 0.0003
π^-	0.325	1895.78 ± 275.34	0.097 ± 0.004	1.110 ± 0.004	0.0080 ± 0.0003
K^+	1.415	63.64 ± 12.60	0.089 ± 0.021	1.128 ± 0.025	0.086 ± 0.009
K^-	1.309	113.82 ± 68.83	0.090 ± 0.012	1.126 ± 0.023	0.085 ± 0.003
p	0.170	10.01 ± 3.71	0.213 ± 0.029	1.026 ± 0.024	0.310 ± 0.190
\bar{p}	0.111	11.62 ± 3.48	0.183 ± 0.015	1.051 ± 0.014	0.437 ± 0.103

TABLE III: χ^2/ndf and different extracted parameters from Tsallis distribution fit(Eq. 8) to the p_T spectra of (a) π^+ , K^+ and p for most peripheral Au+Au collisions and $p + p$ collisions at $\sqrt{s_{NN}} = 200$ GeV; (b) $\frac{\pi^+ + \pi^-}{2}$, $\frac{K^+ + K^-}{2}$ and $\frac{p + \bar{p}}{2}$ for most peripheral Pb+Pb collisions and $\frac{\pi^+ + \pi^-}{2}$, $\frac{K^+ + K^-}{2}$ and $\frac{p + \bar{p}}{2}$ for $p + p$ collisions at $\sqrt{s_{NN}} = 2.76$ TeV.

Au+Au 200 GeV (Peripheral)					
Particle	χ^2/ndf	$V (fm)^3$	$T (GeV)$	β	q
π^+	16.558	302.680 ± 7.591	0.152 ± 0.001	0.475 ± 0.013	1.021 ± 0.004
K^+	2.2461	30.005 ± 1.676	0.154 ± 0.044	0.363 ± 0.008	1.020 ± 0.021
p	0.1825	17.731 ± 1.952	0.247 ± 0.000	0.147 ± 0.018	1.004 ± 0.041
$p + p$ 200 GeV					
π^+	1.370	60.260 ± 0.506	0.123 ± 0.015	0.455 ± 0.015	1.025 ± 0.015
K^+	0.996	7.914 ± 0.878	0.160 ± 0.004	0.400 ± 0.013	1.027 ± 0.038
p	3.144	25.970 ± 0.667	0.194 ± 0.017	0.258 ± 0.019	1.010 ± 0.010

(a)

Pb+Pb 2.76 TeV (Peripheral)					
Particle	χ^2/ndf	$V (fm)^3$	$T (GeV)$	β	q
$\frac{\pi^+ + \pi^-}{2}$	5.657	444.714 ± 7.931	0.185 ± 0.008	0.480 ± 0.028	1.027 ± 0.006
$\frac{K^+ + K^-}{2}$	1.025	149.038 ± 11.465	0.200 ± 0.133	0.460 ± 0.021	1.023 ± 0.010
$\frac{p + \bar{p}}{2}$	0.258	14.507 ± 1.107	0.299 ± 0.090	0.260 ± 0.055	1.013 ± 0.024
$p + p$ 2.76 TeV					
$\frac{\pi^+ + \pi^-}{2}$	18.290	191.039 ± 15.890	0.116 ± 0.003	0.601 ± 0.013	1.038 ± 0.004
$\frac{K^+ + K^-}{2}$	8.006	10.164 ± 1.097	0.197 ± 0.005	0.433 ± 0.016	1.023 ± 0.005
$\frac{p + \bar{p}}{2}$	7.596	1.839 ± 0.256	0.224 ± 0.006	0.310 ± 0.014	1.014 ± 0.004

(b)

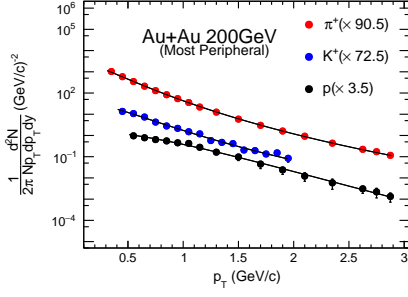


FIG. 11: (color online) Fitting of invariant p_T spectra with Tsallis distribution using Eq. 7 for π^+ [46], K^+ [46], p [46] in most peripheral Au+Au collisions at $\sqrt{s_{NN}}=200$ GeV. Symbols represent the data points and line is the fit function.

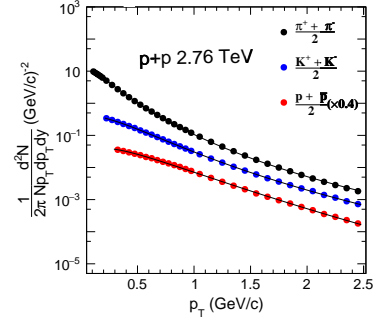


FIG. 14: (color online) Fitting of invariant p_T spectra with Tsallis distribution using Eq. 7 for $\frac{\pi^+ + \pi^-}{2}$ [48], $\frac{K^+ + K^-}{2}$ [48], $\frac{p + \bar{p}}{2}$ [48] in $p + p$ collisions at $\sqrt{s_{NN}}=2.76$ TeV. Symbols represent the data points and line is the fit function.

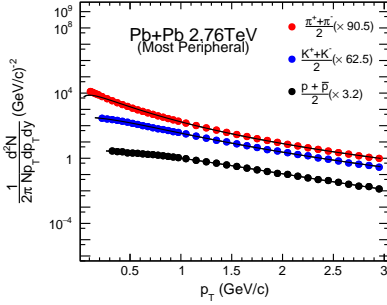


FIG. 12: (color online) Fitting of invariant p_T spectra with Tsallis distribution using Eq. 7 for $\frac{\pi^+ + \pi^-}{2}$ [48], $\frac{K^+ + K^-}{2}$ [48], $\frac{p + \bar{p}}{2}$ [48] in most peripheral Pb+Pb collisions at $\sqrt{s_{NN}}=2.76$ TeV. Symbols represent the data points and line is the fit function.

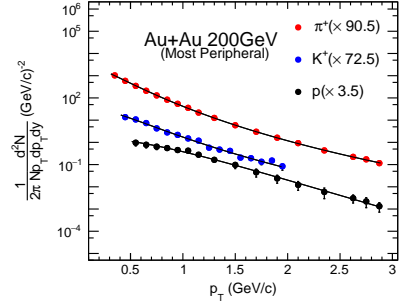


FIG. 15: (color online) Fitting of invariant p_T spectra with Tsallis distribution including chemical potential using Eq.6 for π^+ [46], K^+ [46], p [46] in most peripheral Au+Au collisions at $\sqrt{s_{NN}}=200$ GeV. Symbols represent the data points and the line is the fit function.

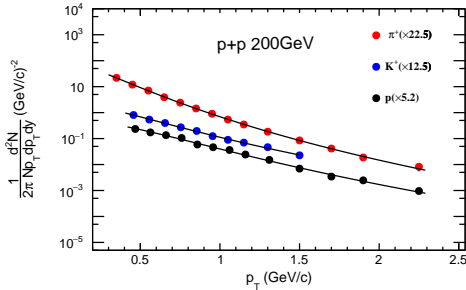


FIG. 13: (color online) Fitting of invariant p_T spectra with Tsallis distribution using Eq. 7 for π^+ [49], K^+ [49], p [49] in $p + p$ collisions at $\sqrt{s_{NN}}=200$ GeV. Symbols represent the data points and line is the fit function.

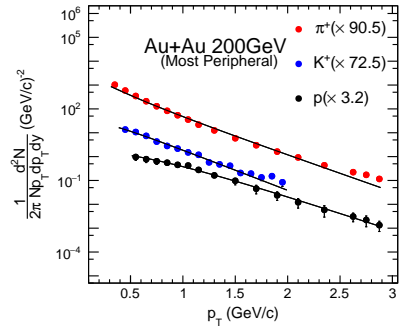


FIG. 16: (color online) Fitting of invariant p_T spectra with Tsallis distribution including radial flow using Eq. 8 for π^+ [46], K^+ [46], p [46] in most peripheral Au+Au collisions at $\sqrt{s_{NN}}=200$ GeV.

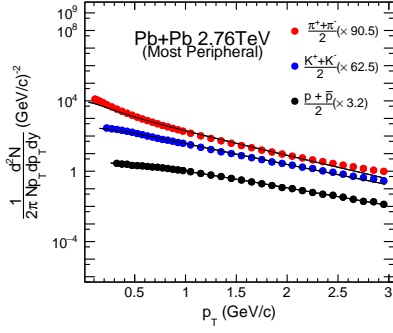


FIG. 17: (color online) Fitting of invariant p_T spectra with Tsallis distribution including radial flow using Eq. 8 for $\frac{\pi^+ + \pi^-}{2}$ [48], $\frac{k^+ + k^-}{2}$ [48], $\frac{p + \bar{p}}{2}$ [48] in most peripheral Pb+Pb collisions at $\sqrt{s_{NN}}=2.76$ TeV; Symbols represent the data points and the line is the fit function.

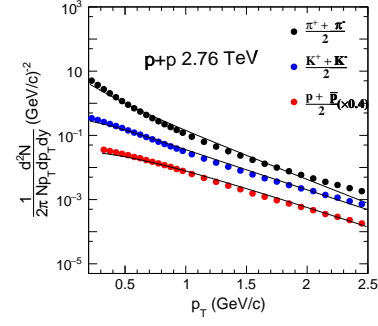


FIG. 19: (color online) Fitting of invariant p_T spectra with Tsallis distribution including radial flow using Eq. 8 for $\frac{\pi^+ + \pi^-}{2}$ [48], $\frac{k^+ + k^-}{2}$ [48], $\frac{p + \bar{p}}{2}$ [48] in $p + p$ collisions at $\sqrt{s_{NN}}=2.76$ TeV. Symbols represent the data points and the line is the fit function.

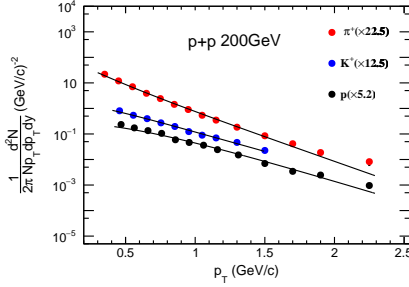


FIG. 18: (color online) Fitting of invariant p_T spectra with Tsallis distribution including radial flow using Eq. 8 for π^+ [49], K^+ [49], p [49] in $p + p$ collisions at $\sqrt{s_{NN}}=200$ GeV. Symbols represent the data points and the line is the fit function.

-
- [1] R. Hagedorn, Nuovo Cim. Suppl. **3**, 147 (1965).
[2] C. Michael and L. Vanryckeghem, J. Phys. G **3** L151 (1977); C. Michael, Prog. Part. Nucl. Phys. **2**, 1 (1979).
[3] G. Arnison *et al.* [UA1 Collab.], Phys. Lett. B **118**, 167 (1982).
[4] R. Hagedorn, Riv. Nuovo Cim. **6N10**, 1 (1983).
[5] B. I. Abelev *et al.* [STAR Collab.], Phys. Rev. C **75**, 064901 (2007).
[6] A. Adare *et al.* [PHENIX Collab.], Phys. Rev. C **83**, 064903 (2011).
[7] K. Aamodt *et al.* [ALICE Collab.], Eur. Phys. J. C **71**, 1655 (2011).
[8] B. Abelev *et al.* [ALICE Collab.], Phys. Letts. B **717**, 162 (2012).
[9] B. Abelev *et al.* [ALICE Collab.], Phys. Letts. B **712**, 309 (2012).
[10] S. Chatrchyan *et al.* [ALICE Collab.], Eur. Phys. J. C **72**, 2164 (2012).
[11] T. Bhattacharyya, P. Garg, R. Sahoo and P. Samantray, Eur. Phys. J. A **52**, 283 (2016).
[12] C. Tsallis, J. Statist. Phys. **52**, 479 (1988).
[13] C. Tsallis, Eur. Phys. J. A **40**, 257 (2009).
[14] C. Tsallis, Introduction to Nonextensive Statistical Mechanics (Springer, 2009).
[15] J. Cleymans and D. Worku, J. Phys. G **39**, 025006 (2012).
[16] D. K. Mishra, P. Garg, P. K. Netrakanti and A. K. Mohanty, J. Phys. G **42**, 105105 (2015).
[17] P. Sett and P. Shukla, Int. J. Mod. Phys. E **24**, 1550046 (2015).
[18] T. Bhattacharyya, J. Cleymans, A. Khuntia, P. Pareek and R. Sahoo, Eur. Phys. J. A **52**, 30 (2016).
[19] H. Zheng and L. Zhu, Adv. High Energy Phys. **2015**, 180491 (2015).

- [20] Z. Tang, Y. Xu, L. Ruan, G. van Buren, F. Wang and Z. Xu, Phys. Rev. C **79**, 051901 (2009).
- [21] B. De, Eur. Phys. J. A **50**, 138 (2014).
- [22] I. Bediaga, E.M.F. Curado, J.M. de Miranda, Physica A **286** (2000) 156.
- [23] S. Tripathy, T. Bhattacharyya, P. Garg, P. Kumar, R. Sahoo and J. Cleymans, Eur. Phys. J. A **52**, 289 (2016).
- [24] A. Khuntia, P. Sahoo, P. Garg, R. Sahoo and J. Cleymans, Eur. Phys. J. A **52**, 292 (2016).
- [25] G. Wilk and Z. Włodarczyk, Acta Phys. Polon. B **46** (2015) 1103.
- [26] K. Ürmösy, G.G. Barnaföldi, T.S. Biró, Phys. Lett. B **701** (2011) 111.
- [27] K. Ürmösy, G.G. Barnaföldi, T.S. Biró, Phys. Lett. B **718** (2012) 125.
- [28] P. K. Khandai, P. Sett, P. Shukla, V. Singh, Int. Jour. Mod. Phys. A **28** (2013) 1350066.
- [29] B.-C. Li, Y.-Z. Wang and F.-H. Liu, Phys. Lett. B **725** (2013) 352.
- [30] L. Marques, J. Cleymans and A. Deppman Phys. Rev. D **91** (2015) 054025.
- [31] B. I. Abelev et al. (STAR collaboration), Phys. Rev. C **75** (2007) 064901.
- [32] A. Adare et al. (PHENIX collaboration), Phys. Rev. D **83** (2011) 052004.
- [33] A. Adare et al. (PHENIX collaboration), Phys. Rev. C **83** (2011) 064903.
- [34] K. Aamodt, et al. (ALICE collaboration), Phys. Lett. B **693** (2010) 53.
- [35] K. Aamodt, et al. (ALICE collaboration), Eur. Phys. J C **71** (2011) 1655.
- [36] V. Khachatryan, et al. (CMS collaboration), J. of High Eng. Phys. **02** (2010) 041;
- [37] V. Khachatryan, et al. (CMS collaboration), Phys. Rev. Lett. **105** (2010) 022002.
- [38] G. Aad, et al. (ATLAS collaboration), New J. Phys. **13** (2011) 053033.
- [39] B. Abelev, et al. (ALICE collaboration), Phys. Rev. Letts. **109** (2012) 252301.
- [40] J. Adams *et al.* (STAR collaboration), Nucl. Phys. A **757** (2005) 102.
- [41] J. Cleymans and M. D. Azmi, Eur. Phys. J C **75** (2015) 430.
- [42] B. C. Li, Z. Zhang, J. H. Kang, G. X. Zhang and F. H. Liu, Adv. High Energy Phys. **2015**, 741816 (2015).
- [43] C. Beck, Physica A **286**, 164 (2000).
- [44] C. Ristea, A. Jipa, O. Ristea, C. Besliu, I. Lazanu, M. Calin, T. Esanu and V. Covlea, EPJ Web Conf. **66**, 04024 (2014).
- [45] V.5.34/32 (June 23 2015), CERN ROOT: <http://root.cern.ch>.
- [46] S. S. Adler *et al.* [PHENIX Collaboration], Phys. Rev. C **69**, 034909 (2004).
- [47] H. R. Wei, F. H. Liu and R. A. Lacey, arXiv:1509.09083 [nucl-ex].
- [48] B. B. Abelev *et al.* [ALICE Collaboration], Phys. Lett. B **736**, 196 (2014) Phys. Rev. Lett. **111**, 222301 (2013).
- [49] J. Adams *et al.* [STAR Collaboration], Phys. Lett. B **616** 8 (2005).
- [50] C. M. Hung and E. Shuryak, Phys. Rev. C **57**, 1891 (1998).
- [51] M. Rybczynski and Z. Wlodarczyk, Eur. Phys. J. C **74**, 2785 (2014).
- [52] S. Chatterjee, S. Das, L. Kumar, D. Mishra, B. Mohanty, R. Sahoo and N. Sharma, Adv. High Energy Phys. **2015**, 349013 (2015). doi:10.1155/2015/349013
- [53] S. Chatterjee, B. Mohanty and R. Singh, Phys. Rev. C **92**, 024917 (2015).
- [54] H. Zheng and L. Zhu, Adv.High Energy Phys. 2016 (2016) 9632126.
- [55] M. Biyajima, T. Mizoguchi, N. Nakajima, N. Suzuki and G. Wilk, Eur. Phys. J. C **48**, 597 (2006).
- [56] T.S. Biró, G. Barnaföldi, P. Ván, Physica A **417** (2015) 215.
- [57] T.S. Biró, P. Ván, G. Barnaföldi, K. Ürmösy, Entropy **16** (2014) 6497.
- [58] Hai-Ling Lao, Hua-Rong Wei, Fu-Hu Liu, and Roy A. Lacey, Eur. Phys. J. A **52**, 203 (2016).